Chapter 2

Literature Review

In this chapter I review the factors that will influence the film morphology of organic molecular crystals, with emphasis on the surface energy of substrates, intermolecular force of organic semiconducting materials consisting of planar molecules. Then listing some successful examples of 1D organic nanostructures. Finally, the field emission theory is introduced to explain the mechanism of electron emitting.

2.1 Thin Film Growth

Thin film growth processes are of tremendous importance for the fabrication of nanostructures and electronic devices. It is therefore essential to understand the microscopic processes involved in thin film growth and especially their effect on the structure of the film.

The growth of an organic molecular thin film on a substrate is strongly influenced by the characteristics of the interface between both materials [69-70]. The film growth is actually a dynamic phenomenon, which involves the flux of adsorbates towards the surface, the adsorption and re-desorption, and the diffusion processes on the surfaces. Figure 2-1 (a) demonstrates the elementary growth processes, e.g. (1) the adsorption, (2) the surface diffusion of monomers or dimers, (3) the island nucleation, (4) the attachment to and detachment from step edges, (5) the diffusion along steps, and (6) the desorption.

Every atomic configuration of the sample corresponds to an energy state, E. If adatom diffuses from a lattice site a, with the energy E_a, to a lattice site b, with the energy E_b, the adatom has to overcome the intermediate states with the energy E^*, as shown in

Figure 2-1 (b). For the diffusion of adatoms on a surface, this is the surface diffusion barrier, E_D. If adatoms diffuse and jump over a step edge, this energy barrier is called as the Ehrlich-Schwoebel barrier [71]. Figure 2-2 illustrates that adatoms diffuse from (a) the lower layer or (b) the upper layer toward a step edge. Owing to in both cases the adatoms have to overcome the Ehrlich-Schwoebel barrier to continue their diffusion, most of them stay at the step edge and form a step bunching and islanding phenomena [72-74].

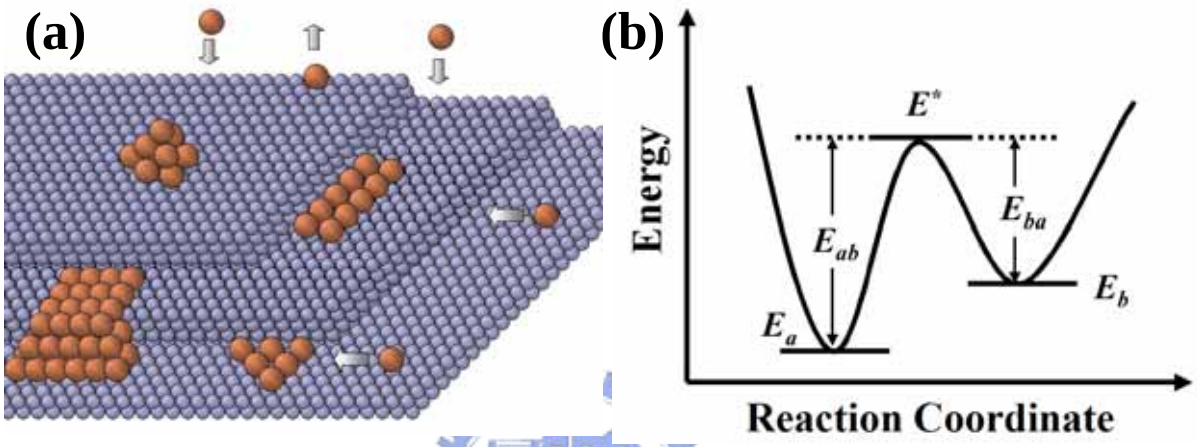

Figure 2-1 *(a) Elementary processes during MBE growth. Atoms from the gas phase adsorb on the surface. There, the monomers diffuse on terraces, incorporate in step edges, form two dimensional and three-dimensional clusters or desorb again into the gas phase. The arrows indicate a selection of possible processes during the deposition.(b) Energy of a system which changes from state a to state b. The energy barriers E_{ab} for the transition a → b and E_{ba} for the transition b → a are indicated, together with the energy E^* of the most unfavored transition state.*

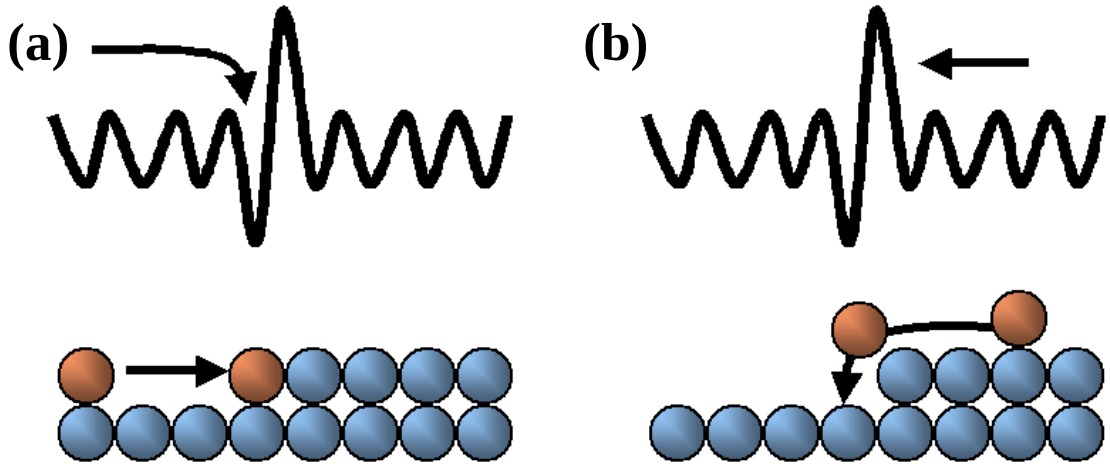

Figure 2-2 *Schematic of the Ehrlich-Schwoebel barrier. (a) Adatoms diffusing from the lower layer to the step edge. (b) Adatoms diffusing from the upper layer to the step edge.*

As the organic molecules deposit on inorganic substrate, owing to the two systems consisted with different size of atoms and different size of the unit cell, each organic molecule will interacts with several atoms of the inorganic substrate, and commonly the lattices of the substrate and the organic layer are incommensurate. According to the definitions of Hooks et al. [75], the unit mesh of the substrate surface is described by two lattice vectors a_1 and a_2, and the adsorbate layer by b_1 and b_2. The transformation between the two lattices is given by

$$\begin{bmatrix} \mathrm{b}_1 \\ \mathrm{b}_2 \end{bmatrix} = [C] \begin{bmatrix} \mathrm{a}_1 \\ \mathrm{a}_2 \end{bmatrix}$$

with the transformation matrix [*C*]. Figures 2-3 shows examples for different epitaxial relationships between the substrate and the adsorbate layer. For a so-called commensurate structure, every lattice point of the adsorbate coincides with a lattice point of the substrate, and therefore all elements of [C] are integers. As for the case of coincident epitaxy, the adsorbate lattice points coincide only partially with substrate lattice points, i.e. that the elements of [C] are rational. If the lattices of the substrate and the adsorbate layer are not related by coincidence, and [C] has at least one irrational element, but no integer, this case is defined as an incommensurate structure. Examples of a commensurate structure are 1,4,5,8-naphthalene-tetracarboxylic-dianhydride (NTCDA) on Ag(111) and Ag(110) [76], of a coincident structure PTCDA on highly-oriented pyrolytic graphite (HOPG) [77], and of an incommensurate structure N,N'-dimethylperylene-3,4,9,10-bis(dicarboximide) (DMPBCDI) on Ag(111) [78].

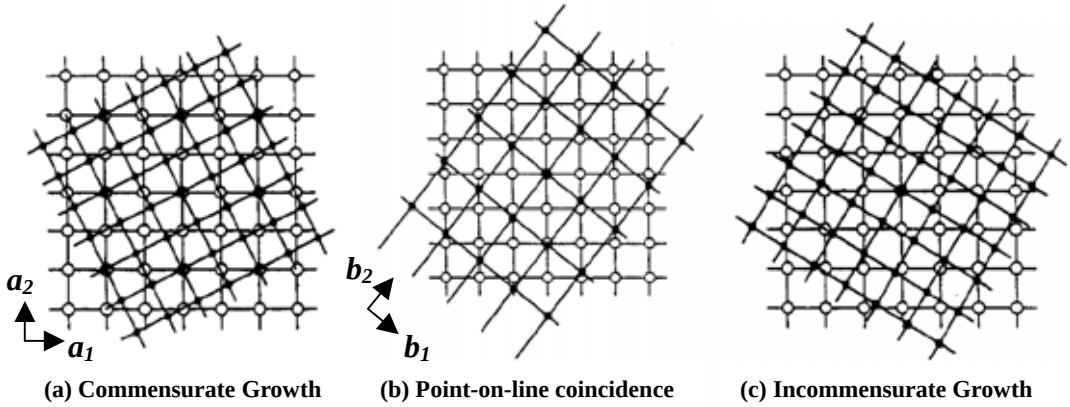

Figure 2-3 *Different types of epitaxial relationships between the two-dimensional lattices of the substrate surface (lattice vectors a_1 and a_2) and an adsorbate layer (lattice vectors b_1 and b_2). (a) Commensurate structure, (b) coincident structure, and (c) incommensurate structure.*

The epitaxy of planar organic molecules is determined by the competition between the adsorbate-substrate interaction and the adsorbate-adsorbate interaction. The adsorbate-substrate interaction varies between weak interaction (physisorption) and strong interaction (chemisorption) [79], depending on the charge transfer between the adsorbate and the substrate. For a better charge conductance, the commensurate or coincident epitaxy is preferred for device application. Several factors favor commensurate or coincident epitaxy are as follows:

- The adsorbate-substrate interaction is weak enough to permit surface diffusion, but dominates the intermolecular interaction.
- The existence of a low-index bulk crystalline plane which coincides with the molecular plane.
- The misfit between a low-index plane of the molecular bulk crystal and the substrate lattice is not too large. Organic over-layers tolerate strain up to approximately 10 %, within the range minor influence will disturb the epitaxy.

The microscopic growth processes discussed above lead to several epitaxial growth modes, as shown in Figure 2-4. These include (a) layer-by-layer growth, also called Frank-van der Merve growth, where one monolayer grows after the other, (b) island growth (Vollmer-Weber growth), where separate islands with several monolayers height develop, and (c) Stransky-Krastanov growth, where the initial layer-by-layer growth is followed by island growth [80, 81]. Due to the requirement for commensurability, it is difficult to find organic molecules/substrate combinations leading to unstrained van der Waals epitaxy; hence Stranski-Krastanov growth tends to be the most frequently observed mode.

In many cases, the first monolayer structure of an organic adsorbate is different from their bulk structures. Considering two scenarios: a monolayer structure similar to the bulk structure, but slightly distorted; and a monolayer structure which differs significantly from the bulk structure. In the first case, the structure can relax to the bulk structure, either directly after the first monolayer [82], or slowly with increasing film thickness [71]. The film is expected to be highly ordered since the unit cell changes only slightly with the film thickness, and the order of the first monolayer is continued. In the second case, since

the monolayer structure differs significantly from the bulk structure, the film is expected to be less ordered. Frequently, organic materials have several bulk polymorphs. In general, the energy differences between the bulk polymorphs are very small, and the structure of the film may change substantially with the growth parameters.

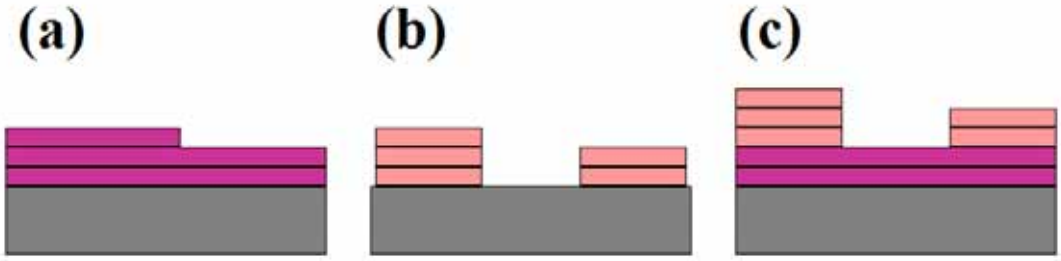

Figure 2-4 *Schematic of the basic growth modes: (a) layer-by-layer growth, (b) island growth, and (c) Stransky-Krastanov growth.*

2.2 Surface Energy

Surface energies of substrate and of adsorbates concern with the interface interaction. These interfacial forces determine whether the film morphology is wetted or dewetted on a substrate. For figuring out the way to synthesize 1D nanostructure, it is crucial to learn more detail on this concept. In this section, I will review the definition and the measuring method of surface energy.

2.2.1 Definition of Surface Energy

Surface energy derives from the unsatisfied bonding potential of molecules at a surface. This is in contrast to molecules within a material, which have less energy because they are subject to interactions with other like molecules in all directions. Molecules at the surface will try to reduce this free energy by interacting with molecules in an adjacent phase. When one of the adjacent phases is a gas, the free energy per unit area is termed the surface energy for solids, and the surface tension for liquids. As the interface between two condensed phase (i.e. solid-solid, solid-liquid and immiscible liquid-liquid interfaces) was concerned, the free energy per unit area of the interface is termed as the interfacial energy. When an adsorbate attaches to a surface in atmosphere, there are three interfacial energies involved: γ_{as} for adsorbate-substrate, γ_{ag} for

adsorbate-gas, and γ_{gs} for substrate-gas. The balance of these interfacial energies is called the free energy of adhesion (F). Therefore $F = \gamma_{as} - \gamma_{ag} - \gamma_{gs}$ [83]. Thermodynamically, adhesion is favored if the free energy of adhesion is negative, i.e. $F < 0$. A high, positive F value is favorable for reducing adhesion. Practically, the interfacial free energy of each of the interfaces can be derived from surface energy measurements of each component in the system. Contact angle measurements can be used to determine the surface energies. The term surface energy is also closely linked with surface hydrophobicity. Whereas surface energy describes interactions with a range of materials, surface hydrophobicity describes these interactions with water only. Because water has a huge capacity for bonding, a material of high surface energy can enter into more interactions with water and consequently will be more hydrophilic. Therefore hydrophobicity generally decreases as surface energy increases. Hydrophilic surfaces such as glass therefore have high surface energies, whereas hydrophobic surfaces such as PTFE or polystyrene have low surface energies.

2.2.2 Wetting

Wetting is the contact between a fluid and a surface, when the two are brought into contact. When a liquid has a high surface tension (strong internal bonds), it will form a droplet, whereas a liquid with low surface tension will spread out over a greater area (bonding to the surface). On the other hand, if a surface has a high surface energy (or surface tension), a drop will spread and wet the surface. If the surface has a low surface energy, a droplet will form. This phenomenon is a result of the minimization of interfacial energy. If the surface is high energy, it will want to be covered with a liquid because this interface will lower its energy, and so on [84].

The primary measurement to determine wettability is a contact angle measurement. This measures the angle between the surface and the surface of a liquid droplet on the surface. For example, a droplet would have a high contact angle, but a liquid spread on the surface would have a small one. The contact angle θ and the surface energies of the materials involved are related by the equation [85]

$$\gamma_{sv} = \gamma_{sl} + \gamma_{lv} \cos\theta \tag{2.1}$$

where γ is the surface tension between two substances and *s*, *v*, and *l* correspond to the solid, vapor, and liquid substances in a contact angle experiment respectively.

A contact angle of 90° or greater generally characterizes a surface as not-wettable, and one less than 90° means that the surface is wettable. In the context of water, a wettable surface may also be termed hydrophilic and a non-wettable surface hydrophobic. Superhydrophobic surfaces have contact angles greater than 150°, showing almost no contact between the liquid drop and the surface. This is sometimes referred to as the "lotus-leaf effect" [86]. This characteristic of spreading out over a greater area is sometimes called “wetting action” when discussing solders and soldering. It is an important factor in the bonding (adherence) of two materials.

2.2.3 Contact Angle and surface energy

In 1805 YOUNG had already formulated a relationship between the interfacial tensions at a point on a 3-phase contact line. Indices *s* and *l* stand for “solid” and “liquid”; the symbols σ_s and σ_l describe the surface tension components of the two phases; symbol γ_{sl} represents the interfacial tension between the two phases, and θ stands for the contact angle corresponding to the angle between vectors σ_l and γ_{sl}. YOUNG formulated the following relationship between these quantities:

$$\sigma_s = \gamma_{sl} + \sigma_l \cdot \cos\theta \tag{2.2}$$

According to this formula, one can determine the surface energy of solids from contact angle data. They are mainly based on combining various starting equations for γ_{sl} with the equation from YOUNG to obtain equations of state, in which $\cos\theta$ represents a function of the phase surface tensions and, if applicable, the polar and disperse tension components $\sigma_{l,}^{D}$, $\sigma_{l,}^{P}$, $\sigma_{s,}^{D}$, $\sigma_{s,}^{P}$. For liquids with known surface tension data and known polar and disperse fractions, it is possible to include $\sigma_{l,}^{D}$ and $\sigma_{l,}^{P}$, in the equations. All methods assume that the interactions between the solid and the gas phase are so small as to be negligible. These methods are described in the following sections.

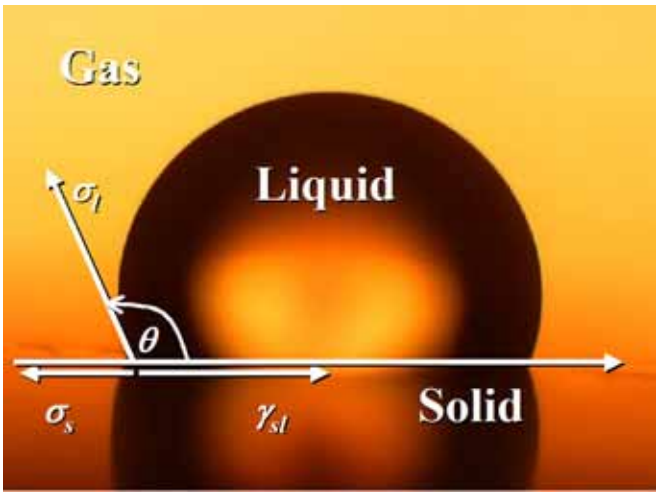

Figure 2-5 *Contact angle of a liquid on a solid surface. The symbols σ_s and σ_l describe the surface tension components of the two phases; symbol γ_{sl} represents the interfacial tension between the two phases.*

2.2.3.1 The ZISMAN method

In the ZISMAN method the surface energy of the solid is determined by using the critical surface tension of the liquid [87]. The method is based on the following consideration: A liquid wets a solid completely when the work of cohesion for the formation of a liquid surface $W_{//}$ is smaller than the work of cohesion for the formation of the interface boundary W_{sl}. The difference between these two quantities is known as the spreading pressure, $S_{l|s} = W_{sl} - W_{//}$. The solid will be wetted completely when the spreading pressure is positive; at a negative spreading pressure the solid will not wetted completely. In addition, the following relationship exists between the work of cohesion W_{sl}, the contact angle θ and the surface tension of the liquid:

$$W_{sl} = \sigma_l(\cos\theta + 1) \tag{2.3}$$

As the work of cohesion $W_{//}$ is defined as $2\sigma_l$, for a contact angle of 0° ($\cos\theta = 1$), the work of cohesion will be the same as the work of adhesion; this results in a spreading pressure of 0. This means that the contact angle of 0° can be called the limiting angle for spreading (complete wetting). Theoretically a positive spreading pressure corresponds with negative contact angles, which cannot be measured in practice. The method according to ZISMAN uses this relationship by plotting $\cos\theta$ against the surface tension for various liquids and extrapolating the compensation curve to $\cos\theta = 1$. The corresponding value

for the surface tension is known as the critical surface tension σ_{crit}. ZISMAN equates this value with the surface energy of the solid σ_s. Setting up a linear relationship between $\cos\theta$ and the surface tension σ_l is based on the assumption that the interfacial tension is determined by the difference between the surface tensions. In fact this linear relationship only applies when the relationship between the dispersal and polar interactions is the same between the solid and the liquid. This practically only occurs when a purely disperse interactive solid and liquid are involved; i.e. only under exceptional circumstances. This means that other methods should normally be used for determining the surface energy.

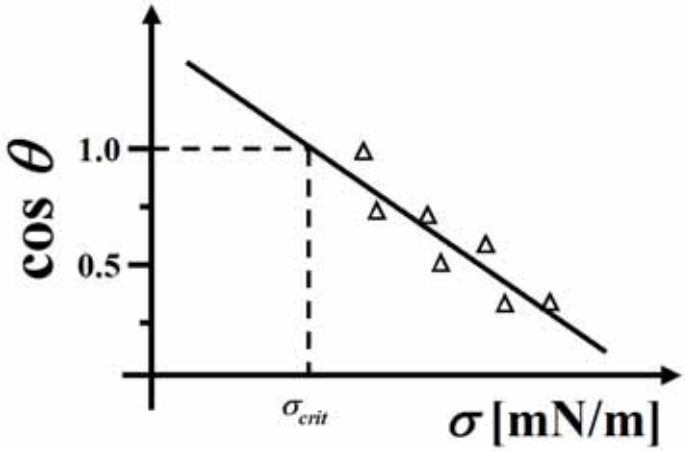

Figure 2-6 *Schematic diagram of the way to determine the critical surface tension according the ZISMAN method.*

2.2.3.2 Equation of State

The equation of state was obtained during the search for a method of determining the surface energy of a solid from a single contact angle measurement by using a liquid with known surface tension [88]. Starting with the equation of Young, $\sigma_s = \gamma_{sl} + \sigma_l \cdot \cos\theta$, it can be seen that a second equation is required which describes the surface energy (σ_s) of the solid as a function of the interfacial tension (γ_{sl}) of solid/liquid and the surface tension (σ_l) of the liquid; $\sigma_s = f(\gamma_{sl}, \sigma_l)$. By using an enormous volume of contact angle data, the equation of state was determined empirically:

$$\gamma_{sl} = \sigma_l + \sigma_s - 2\sqrt{\sigma_l \cdot \sigma_s} \cdot e^{-\beta(\sigma_l - \sigma_s)^2} \qquad (2.4)$$

The constant β in the exponent was determined to be 0.0001247. If the equation of state is

inserted into Young's equation then a new equation is obtained which allows the calculation of the surface tension of the solid σ_s from a single contact angle if the surface tension σ_l is known.

$$\cos\theta = -1 + 2\sqrt{\frac{\sigma_s}{\sigma_l}}e^{-\beta(\sigma_l-\sigma_s)^2} \tag{2.5}$$

In the calculation of the surface energy with the help of the equation of state, the type of interactions which lead to the formation of the interfacial tensions (polar or disperse interactions) are not taken into account. However the assumption that the knowledge of the surface tension of the liquid alone is sufficient has been disproved by experiments in which the contact angles of liquids with similar high surface tensions and differing fractions of polar interactions were measured. It appears that the disperse and polar fractions of the surface tensions must be taken into account; this means that the equation of state only provides useful results when only disperse interactions are present or when these are in the majority.

2.2.3.3 The FOWKES method

By using the FOWKES method the polar and disperse fractions of the surface free energy of a solid can be obtained [88]. Strictly speaking, this method is a combination of the knowledge of FOWKES method and the OWENS, WENDT, RABEL and KAELBLE [89]. As FOWKES initially determined only the disperse fraction and the later were to determine both the components of the surface energy. The different between the FOWKES method and the OWENS, WENDT, RABEL and KAELBLE method is that in the FOWKES method, the disperse and the polar fractions are determined in succession, i.e. in two steps, while in the OWENS, WENDT, RABEL and KAELBLE method both components are calculated by using a single linear regression. The method is as followed:

Step1: Determining the disperse fraction

In the first step the disperse fraction of the surface energy of the solid is calculated by making contact angle measurements with at least on purely disperse liquid. By combination of the surface tension equation of FOWKES for the disperse fraction of the

interactions

$$\gamma_{sl} = \sigma_s + \sigma_l - 2\sqrt{\sigma_s^D \cdot \sigma_l^D} \tag{2.6}$$

with the YOUNG equation, the following equation for the contact angle is

$$\cos\theta = 2\sqrt{\sigma_s^D} \cdot \frac{1}{\sqrt{\sigma_l^D}} - 1 \tag{2.7}$$

Based upon the general equation for a straight line, $y = mx + b$, $\cos\theta$ is then plotted against the term $1/\sqrt{\sigma_l}^D$, and $2\sqrt{\sigma_s}^D$ can be determined from the slope m. The straight line must intercept the ordinate at the point defined as b = -1. As this point has been defined, it is possible to determine the disperse fraction from a single contact angle; however a linear regression with several purely disperse liquids is more accurate.

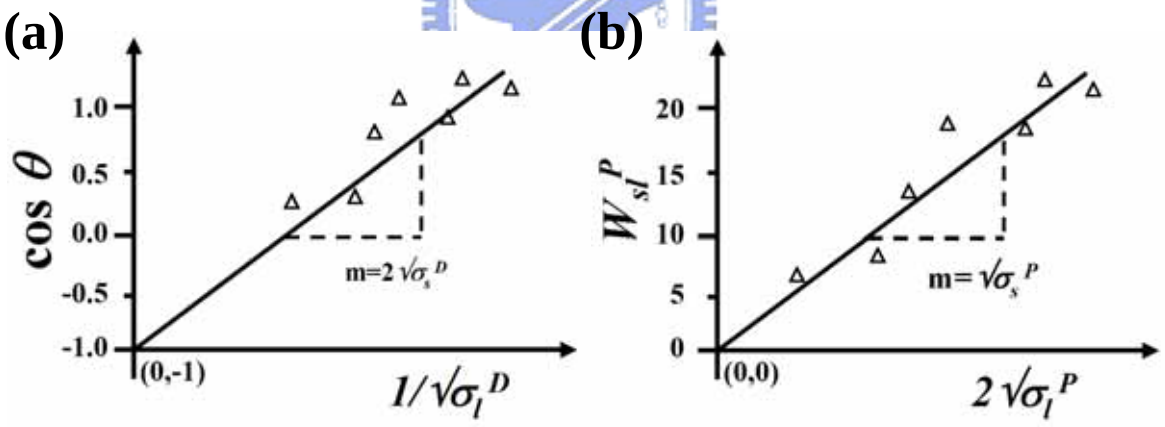

Figure 2-7 *Schematic diagram of the way to determine (a) the disperse fraction of surface energy and (b) the polar fraction of surface energy according the FOWKES method.*

Step2: Determining the polar fraction

For the second step, the calculation of the polar fraction Equation (2.6) is extended by the polar fraction:

$$\gamma_{sl} = \sigma_s + \sigma_l - 2\left(\sqrt{\sigma_s^D \sigma_l^D} + \sqrt{\sigma_s^P \sigma_l^P}\right) \tag{2.8}$$

It is assumed that the work of adhesion is obtained by adding together the polar and disperse fractions:

$$W_{sl} = W_{sl}^D + W_{sl}^P \tag{2.9}$$

and then as a third step, the work of adhesion, $W_{sl} = \sigma_l(\cos\theta + 1)$ and DUPRE equation, $W_{sl} = \sigma_s + \sigma_l - \gamma_{sl}$ are taken into account. A combination of these equations leads to the polar faction of the surface energy:

$$W_{sl}^P = \sigma_l(\cos\theta + 1) - 2\sqrt{\sigma_s^D \cdot \sigma_l^D} \tag{2.10}$$

Based upon this relationship the contact angles of liquids with known polar and disperse fractions are measured, and $W_{sl}{}^P$ is calculated for each liquid. In this case a single liquid with polar and disperse fractions would be sufficient, although the results would again be less reliable. As according to Equation (2.8) the polar fraction of the work of adhesion is defined by the geometric mean of the polar fractions of the particular surface tensions.

$$W_{sl}^P = 2\sqrt{\sigma_l^P \cdot \sigma_s^P} \tag{2.11}$$

then, by plotting $W_{sl}{}^P$ against $2\sqrt{\sigma_l}^P$ and following this with a linear regression, the polar fraction of the surface energy of the solid can be determined from the slope. As in this case, the ordinate intercept *b* is 0; the regression curve must pass through the origin (0,0).

2.2.3.4 The OWENS, WENDT, RABEL and KAELBLE method

According to OWENS, WENDT, RABEL and KAELBLE [89], the surface tension of each phase can be split into a polar and a disperse fraction, i.e. $\sigma_l = \sigma_l^P + \sigma_l^D$ and $\sigma_s = \sigma_s^P + \sigma_s^D$. In contrast to the FOWKES method, in the OWENS, WENDT, RABEL and KAELBLE method the calculation of the surface energy of the solid takes place in a

single step. OWENS and WENDT solved the equation system by using the contact angles of two liquids with known disperse and polar fractions of the surface tension. KAELBLE solved the equation for combinations or two liquids and calculated the mean values of the resulting values for the surface energy. RABEL made it possible to calculate the polar and disperse fractions of the surface energy with the aid of a single linear regression from the contact angle data of various liquids. He combined Equations (2.2) and (2.8) and adapted the resulting equation by transposition to the general equation for a straight line, $y = mx + b$; the transposed equation is shown below:

$$\underbrace{\frac{(1+\cos\theta)\cdot\sigma_l}{\sqrt{\sigma_l^D}}}_{y} = \underbrace{\sqrt{\sigma_s^P}}_{m}\cdot\underbrace{\sqrt{\frac{\sigma_l^P}{\sigma_l^D}}}_{x} + \underbrace{\sqrt{\sigma_s^D}}_{b} \tag{2.12}$$

In a linear regression of the plot of y against x, σ_s^P is obtained from the square of the slope of the curve m and σ_s^D from the square of the ordinate intercept b.

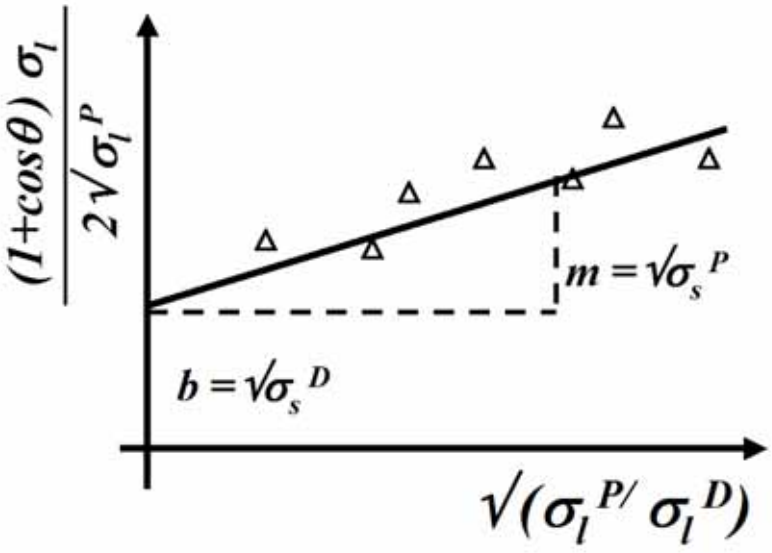

Figure 2-8 *Schematic diagram of the way to determine the disperse and polar fraction of surface energy of a solid according the RABEL method.*

2.2.3.5 The WU method

WU also started with the polar and disperse fractions of the surface energy of the participating phases [90]. However, in contrast to FOWKES and OWENS, who used the

geometric mean of the surface tensions in their calculations, WU used the harmonic mean. In this way he achieved more accurate results, in particular for high-energy systems. At least two test liquids with known polar and disperse fractions are required for this method; at least on of the liquids must have polar fraction >0.

WU's initial equation for the interfacial tension between a liquid and a solid phase is as follows:

$$\gamma_{sl} = \sigma_l + \sigma_s - 4\left(\frac{\sigma_l^D \cdot \sigma_s^D}{\sigma_l^D + \sigma_s^D} + \frac{\sigma_l^P \cdot \sigma_s^P}{\sigma_l^P + \sigma_s^P}\right) \tag{2.13}$$

If YOUNG's equation is inserted in this Equation, then the following relationship is obtained:

$$\sigma_l(\cos\theta + 1) - 4\left(\frac{\sigma_l^D \cdot \sigma_s^D}{\sigma_l^D + \sigma_s^D} + \frac{\sigma_l^P \cdot \sigma_s^P}{\sigma_l^P + \sigma_s^P}\right) = 0 \tag{2.14}$$

In order to determine the two required quantities σ_s^D and σ_s^P, WU determined the contact angles for each of two liquids on the solid surface and then, based on Equation (2.14), he drew up an equation for each liquid. After a factor analysis the resulting equations were as follows:

$$(b_1 + c_1 - a_1)\cdot\sigma_s^D \cdot \sigma_s^P + c_1(b_1 - a_1)\cdot\sigma_s^D + b_1(c_1 - a_1)\cdot\sigma_s^P - a_1 b_1 c_1 = 0 \tag{2.15}$$

$$(b_2 + c_2 - a_2)\cdot\sigma_s^D \cdot \sigma_s^P + c_2(b_2 - a_2)\cdot\sigma_s^D + b_2(c_2 - a_2)\cdot\sigma_s^P - a_2 b_2 c_2 = 0 \tag{2.16}$$

The variables a_1, b_1, c_1 for the first liquid and a_2, b_2, c_2 for the second liquid express the following terms:

$$a_1 = \frac{\sigma_{l,1}(\cos\theta_1 + 1)}{4} \qquad a_2 = \frac{\sigma_{l,2}(\cos\theta_2 + 1)}{4}$$

$$b_1 = \sigma_{l,1}^{D} \qquad b_2 = \sigma_{l,2}^{D}$$

$$c_1 = \sigma_{l,1}^{P} \qquad c_2 = \sigma_{l,2}^{P}$$

The solution of the equations produces the surface energy of the solid σ_s and its polar and disperse components σ_s^P and σ_s^D. However, the following point must be taken into consideration: as quadratic equations are involved this means that two solutions are obtained for both σ_s^P and σ_s^D only one of these solutions describes the actual surface energy.

2.3 Intermolecular Forces

Molecular crystals differ from other classes of solids in being made up of discrete molecules. Although intramolecular forces are strong, intermolecular forces are generally weaker and short-range in their effect. This mixture of strong and weak forces introduces diversity to the properties of molecular crystals. Intramolecular forces determine the most effective ways of packing the molecules together in the crystal. However, if the intermolecular forces are large or strongly dependent on the relative orientation of adjacent molecules, they may modify the crystal structure deduced from simple considerations of molecular packing. An understanding of the origins and magnitudes of intermolecular forces, and their dependence on molecular properties and intermolecular separation and orientation, is therefore essential background for understanding many properties of molecular crystals.

Intermolecular forces can be loosely classified into three categories [15]. First, there are those that are purely electrostatic in origin arising form the Coulomb force between charges. The interactions between charges, permanent dipoles, quadruples, etc., fall into this category. Second, there are polarization forces that arise from the dipole moments induced in atoms, and molecules by the electric fields of nearby charges and permanent dipoles. Third, there are forces that give rise to covalent bonding and to the repulsive interactions that balance the attractive forces at very short distances. Following sections introduce the intermolecular forces that exist commonly in organic crystal.

2.3.1 Interaction between dipolar molecules

The electric field produced by a dipole μ along its own direction and at a distance r from its center is $2\mu/r^3$. Hence, for two dipoles aligned head to tail at a distance r apart, the interaction energy U is given by the product of the magnitude of each dipole and the field at its center produced by the other dipole [91], i.e.

$$U = -2\mu_1\mu_2 / r^3 \tag{2.17}$$

In general the dipoles will not be in this ideal orientation by rather in random orientations specified by polar coordinates θ_1, ϕ_1 and θ_2, ϕ_2, respectively, as shown in Figure 2-9. In considering this situation, a simple starting point is to use the components of the field of dipole 1 at dipole 2 in the z-direction (F_{para}) and perpendicular to the z-direction in a plane containing the direction of μ_1 and the z-axis (F_{perp}), which are given by [92]

$$F_{para} = 2\mu_1 \cos\theta_1 / r^3 \quad \text{and} \quad F_{prep} = \mu_1 \sin\theta_1 / r^3 \tag{2.18}$$

Now, the component of μ_2 in the z-direction is $\mu_2\cos\theta_2$, so there is an attractive force

$$U_{att} = -F_{par}\mu_2 \cos\theta_2 = -2\mu_1\mu_2 \cos\theta_1 \cos\theta_2 / r^3$$

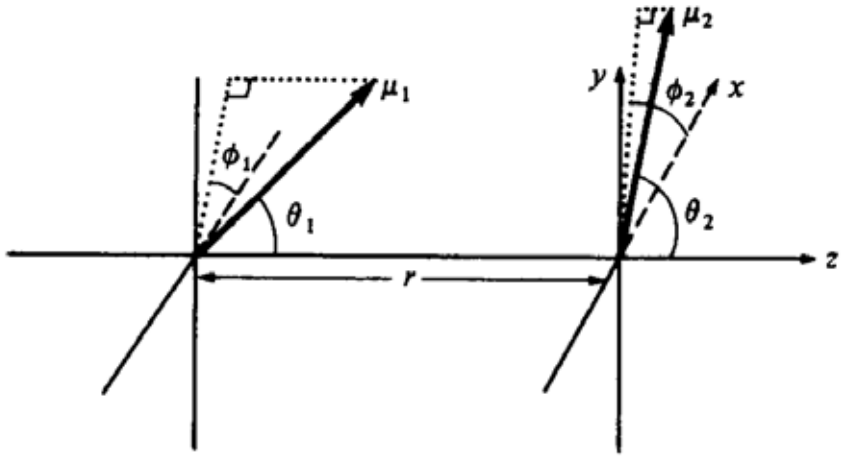

Figure 2-9 *Dipoles in radom orientations specified by polar coordinates θ_1, ϕ_1 and θ_2, ϕ_2, respectively [15].*

However, both dipoles have parallel components, which lie perpendicular to the z-direction and in the plane defined above, and these interact repulsively. The component of μ_2 in this direction is $\mu_2 \sin\theta_2 \cos(\phi_2 - \phi_1)$, so the repulsive force is

$$U_{rep} = (\mu_1 \mu_2 / r^3) \sin\theta_1 \sin\theta_2 \cos(\phi_2 - \phi_1) \tag{2.19}$$

and the net interaction is given by

$$U = -(\mu_1 \mu_2 / r^3)\{2\cos\theta_1 \cos\theta_2 - \sin\theta_1 \sin\theta_2 \cos(\phi_1 - \phi_2)\} \tag{2.20}$$

Hence, for two dipolar molecules held in fixed relative orientations in a crystal, the dipole-dipole interaction energy is proportional to r^{-3}.

2.3.2 Dipole-induced dipole interactions

The electric field ($F = 2\mu_1/r^3$) of one dipole, whose component along the line joining it to a second polarisable molecule centered at a distance r away is μ_1, induces a dipole on this second molecule given by [93]

$$\mu_{ind} = -\alpha_2 F = -2\alpha_2 \mu_1 / r^3 \tag{2.21}$$

where α_2 is the molecular polarisability.

The interaction energy of the permanent dipole with this induced dipole is thus

$$U = F\mu_{ind} = -4\alpha_2 \mu_1^2 / r^6 \tag{2.22}$$

This interaction is always attractive irrespective of the relative orientation of the two molecules, although its magnitude may depend on this orientation if the molecule being polarized has an anisotropic polarisability. Since polar molecules may also be polarized, this interaction also contributes to the total interaction energy of two dipolar molecules, i.e

$$2U_{total} = U_{dipole-dipole} + \sum U_{dipole-induced\_dipole} \tag{2.23}$$

2.3.3 Dispersion forces

Interactions involving permanent dipoles do not explain the cohesive forces holding together crystals composed of non-polar molecules, e.g. anthracene, coronene. London developed the theory of dispersion forces as follows [94]. Consider two spherically symmetrical species with polarisability α, and make small charge displacements $\boldsymbol{r}_1$ (=x_1 y_1 z_1) and $\boldsymbol{r}_2$ (=x_2 y_2 z_2) on each, leading to the formation of dipolar species. The total potential energy is then the sum of the energy required to produce the charge displacements (*I*) and the energy of interaction of the two resulting dipoles (*II*):

$$V = \underbrace{e^2 r_1^2 / 2\alpha + e^2 r_2^2 / 2\alpha}_{I} + \underbrace{(e^2 / r^3)(x_1 x_2 + y_1 y_2 - 2z_1 z_2)}_{II} \tag{2.24}$$

If the displacements are now re-defined in terms of normalized coordinates ($x_+ = (x_1+x_2)/\sqrt{2}$; $x_- = (x_1-x_2)/\sqrt{2}$; $y_+ = (y_1+y_2)/\sqrt{2}$, etc.), the potential-energy expression becomes

$$V = (e^2 / 2\alpha)[(1+\alpha r^{-3})(x_+^2 + y_+^2) + (1-\alpha r^{-3})(x_-^2 + y_-^2) + (1-2\alpha r^{-3})z_+^2 + (1+2\alpha r^{-3})z_-^2 \tag{2.25}$$

which is a sum of squares representing the potential energy of six independent oscillators with frequencies ν_{x+}, ν_{y+}, ν_{z+}, ν_{x-}, ν_{y-}, ν_{z-} given by

$$\begin{aligned} \nu_{x+} &= \nu_{y+} = \nu_0 \sqrt{(1 \pm \alpha\, r^{-3})} \approx \nu_0 \left\{1 \pm (\alpha / 2r^3) - (\alpha^2 / 8r^6) \pm \cdots\right\} \\ \nu_{z+} &= \nu_0 \sqrt{(1 \mp 2\alpha\, r^{-3})} \approx \nu_0 \left\{1 \mp (\alpha / r^3) - (\alpha^2 / 2r^6) \mp \cdots\right\} \end{aligned} \tag{2.26}$$

where $\alpha < r^3$

$\nu_0 = e/(\sqrt{m\alpha})$ and m = reduced mass of each species.

The lowest energy of this system of six oscillators is given by

$$\begin{aligned} E_0 &= (h/2)(\nu_{x+} + \nu_{y+} + \nu_{z+} + \nu_{x-} + \nu_{y-} + \nu_{z-}) \\ &= (h\nu_0 / 2)\left[6 + (\frac{1}{2} + \frac{1}{2} - 1 - \frac{1}{2} - \frac{1}{2} + 1)(\alpha / r^3) - \{(4/8) + (2/2)\}(\alpha^2 / r^6) + \cdots\right] \\ &= 3h\nu_0 - (3/4)h\nu_0 \alpha^2 r^{-6} + \cdots \end{aligned} \tag{2.27}$$

The term $3h\nu_0$ is the zero-point energy of the two isolated species, while the second term $-(3/4)h\nu_0\alpha^2 r^{-6}$ is the attractive dispersion energy. The frequency ν_0 is a characteristic frequency for one of the isolated species and also appears as the frequency at which refractive dispersion increases rapidly, which is why the name "dispersion force" is used.

In practice, more complex charge displacements giving rise to quadrupole and higher multipoles are strictly required for a full description of the state of a molecule, so that the dispersion force should be written as

$$U_{dispersion} = c_6 r^{-6} + c_8 r^{-8} + c_{10} r^{-10} + \cdots \tag{2.28}$$

where c_6, c_8, etc. are constants.

Dipole-dipole, dipole-induced dipole and dispersion forces are often referred to collectively as van der Waals forces. The expressions for their magnitudes discussed above show that van der Waals forces should be largest between polar or polarisable molecules. In fact, contrary to common intuitive impressions, dispersion forces can often be comparable in magnitude with dipole-dipole interactions. Comparison of *o*-xylene and cyclooctatetraene, both containing eight carbon atoms, shows that cyclooctatetraene, which has more polarisable π-electrons, has the higher melting point. Similarly, benzene has a higher melting point than *n*-hexane. The size of the π-electron system increases, the polarisability increases and hence the melting point also increases [95].

2.3.4 Repulsive forces

The closest distance for approaching two molecules is determined by the point at which the attractive forces are exactly balanced by the repulsive forces that arise when the electron clouds of two molecules begin to penetrate each other significantly. These repulsive forces have two main origins. It follows from the Pauli principle that two electrons can occupy the same volume element of space only if they have sufficiently different velocities. This implies that energy must be given to electrons in the region of interpenetration, which is one origin of repulsive forces. Secondly, since electrons will therefore tend to avoid the region of interpenetration, they no longer screen the nuclear

charges on the molecules so effectively and columbic repulsion between nuclei on the two molecules increases. The most commonly used repulsive potentials have the forms [15]:

ar^{-n} (with n commonly 12) and be^{-cr} (2.29)

where a, b, c and n are empirical constants.

The former expression is widely used and has the advantage of simplicity, although the latter one is considered ultimately more realistic. Both these expressions assume isotropic repulsions between atoms, whereas chemists have long realized that in many cases lone-pairs of electrons, d-orbitals, etc. lead to pronounced anisotropy in atomic interactions.

2.4 One Dimensional Organic Nanostructures

The subtle balance among dispersion force, repulsion force and interfacial force determines the film morphology of planar organic materials. The aim of this thesis is to synthesize 1D nanostructures of organic semiconductor materials and evaluate the feasibility as electron emitters. In order to inspire my work and make some necessary comparisons, here I list some examples that have been achieved by other research groups.

2.4.1 AlQ_3 nanowires

Tris(8-hydroxyquinoline)aluminum (AlQ_3) has been one of the most attractive electron transport and emitting materials for OLED devices since the discovery of its strong electroluminescence and low driving voltage by Tang and VanSlyke in 1987 [96]. At the beginning of 2003, Chiu et al. demonstrated its 1D nanostructures by sublimed AlQ_3 powder from a heated graphite boat onto ITO substrate that was mounted on a liquid nitrogen cold trap, which consisted of a cylindrical Pyrex vessel sandwiched by two stainless steel plates [97]. AlQ_3 nanobelts were formed on the substrate first, and then a thick layer of dendritic nanowires was grown above the nanobelts. Figures 2-10 show the TEM images of 1D AlQ_3 nanostructures, i.e. an amorphous nanowire with diameter range from 30 to 50 nm, and a nanobelt with diameter range from 40 to 60 nm were presented. The AlQ_3 nanowires exhibit a turn-on field of 10 V/μm, and the maximum current density is larger than 15 mA/cm^2 at an applied field of 22 V/μm. This study is brilliant for it is

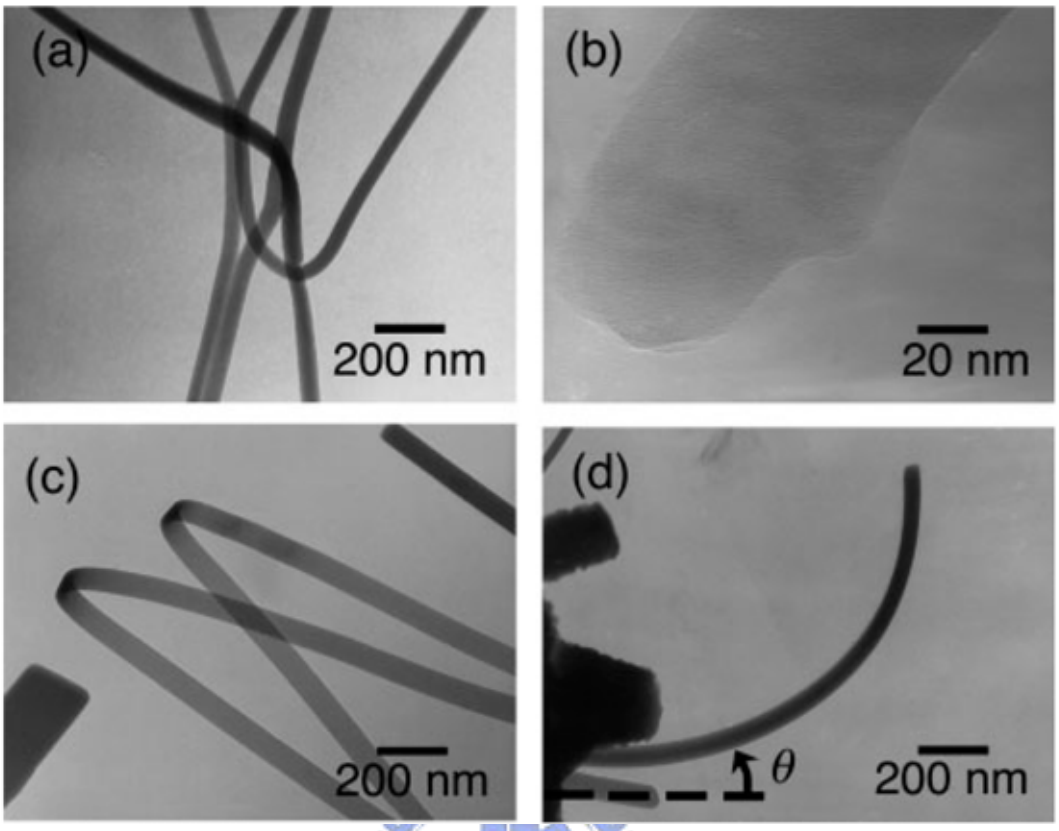

Figure 2-10 *TEM images of the AlQ_3 nanostructures, (a) TEM image of the AlQ_3 nanowires with a diameter of about 30-50 nm. (b) HRTEM image of a typical AlQ_3 nanowire. (c) TEM image of the AlQ_3 nanobelts with a width of about 40–60 nm. (d) An AlQ_3 nanobelt rolls up along the axial direction after irradiated by the electron beam in TEM. The rolling angle increase as the current density increases. [97]*

the first report that reveals the electron-emitting phenomenon of organic semiconductor materials. However, the synthesis process involves pumping down chamber first, then introduce the Ar to collide with the reactant vapor, and finally condense the reactant by liquid nitrogen cold trap. These complicated processes made the reactor hard to design, hence increase the cost of assembling such a reaction chamber.

2.4.2 Anthracene (AN) nanowires and perylene (PY) nanorods

Later in the midterm of 2003, Liu et al. demonstrated the 1D nanostructures of anthracene and perylene, which were synthesized by solid phase organic reaction under controlled reaction temperature, time, and argon gas flow rate [98]. In their work, the organic materials were placed on metal oxide substrates and inserted into a horizontal tube furnace. Figure 2-11 shows the anthracene nanowires with lengths in the range of several

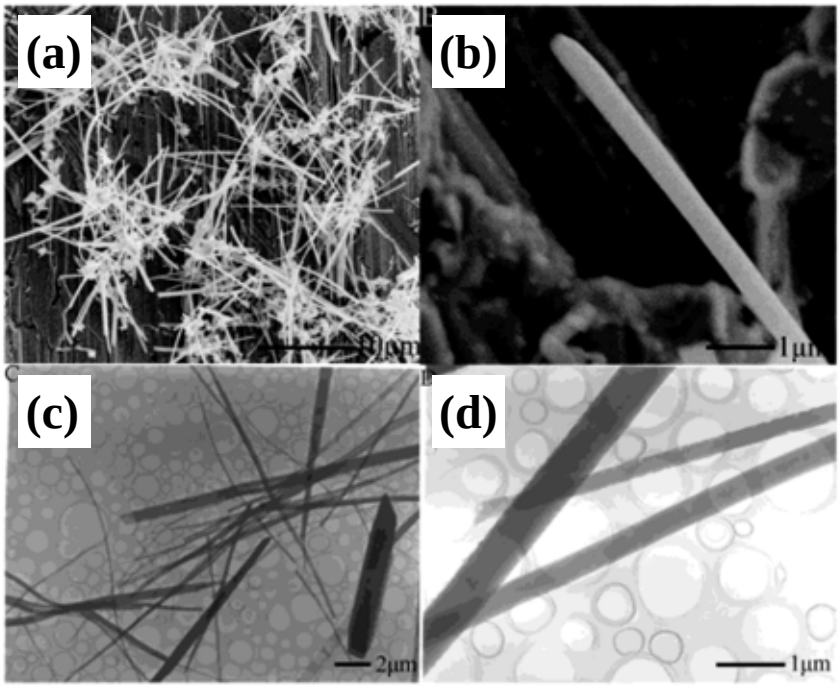

Figure 2-11 *(a) SEM image of the AN nanostructures, (b) SEM image of typical single AN nanowire, (c) Low magnification TEM image of the AN nanostructures, and (d) TEM image of typical AN nanowires. [98]*

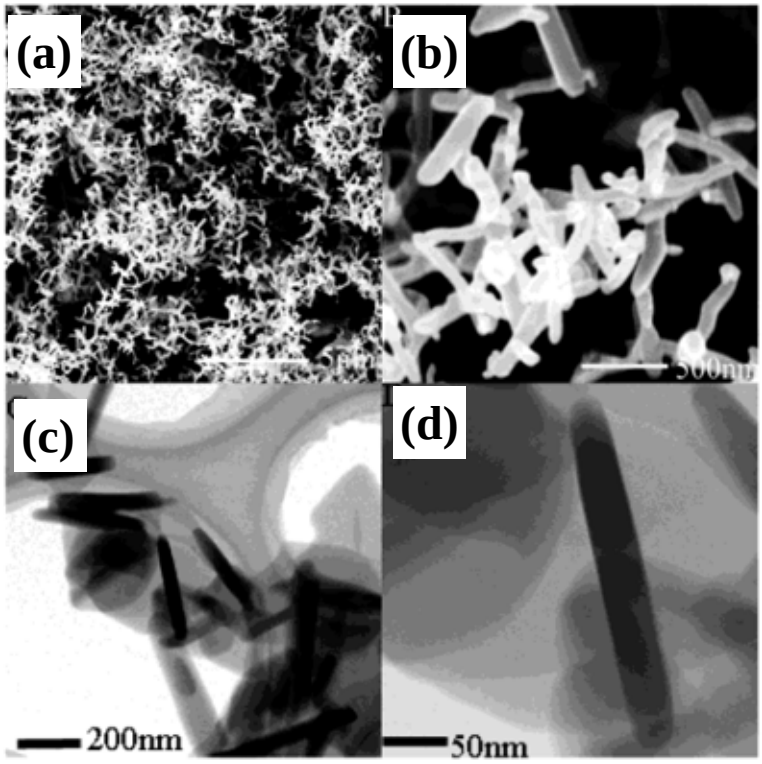

Figure 2-12 *(a) SEM image of the perylene nanostructures, (b) SEM image of perylene nanorods, (c) Low magnification TEM image of the perylene nanorods, and (d) TEM image of a typical perylene nanorod. [98]*

to tens of micrometers, while their diameters are in the range of tens of nanometers to several micrometers. The aspect ratio corresponding nanowires lies in the range of about 50-100. With a similar approach, they also synthesized perylene nanorods with length of hundreds nanometers to several micrometers, while the diameters are in the range of tens nanometers to hundreds nanometers, as shown in Figure 2-12. Despite the successful synthesis of organic 1D nanostructures, the high process temperature (340 °C) and long process time (2 hours) consume considerable thermal budget and limit their application. Moreover, those 1D nanostructures were grown on poor-conductive metal oxides that are not suitable to measure the field emission and carrier conductivity along the 1D nanostructure directly.

2.4.3 AgTCNQ and CuTCNQ nanowires

In 2005, Liu et al. utilized organic vapor-solid-phase reaction to synthesize another 1D organic nanostructures, which were composed of charge-transfer complexes, namely AgTCNQ and CuTCNQ (TCNQ=7,78,8-tetracyanoquinodimethane) [99]. These nanowires were synthesized by loading TCNQ powders in a ceramic boat and then placed at the center of a quartz tube that was inserted into a horizontal tube furnace. The copper or silver foil was placed on top of the ceramic boat. With moderate heating process (120-150 °C), the TCNQ were deposited on the surface of the metal foil for formation of AgTCNQ and CuTCNQ nanowires. Figure 2-13 (a) shows the AgTCNQ nanowires with lengths in the range of several tens of micrometers, and the diameters are in the range of 45-150 nm. As for the CuTCNQ nanowires, the diameter is smaller at the tip position than that at the bottom position, whose diameter of the nanowires tip is in the narrow range of 40-70 nm as shown in Figure 2-13 (b). Owing to these nanowires were synthesized directly on the metal foil, the field emission characteristic can be measured directly. Impressively, the AgTCNQ and CuTCNQ nanowires films exhibit a turn-on field of 2.58 and 3.13 V/μm, which is competitive with CNTs and other inorganic emitters. These values are the lowest values reported so far for electron field emission of organic nanostructures. As compared with other emitters, the low-temperature synthesis condition provides a great potential in electron emitting application.

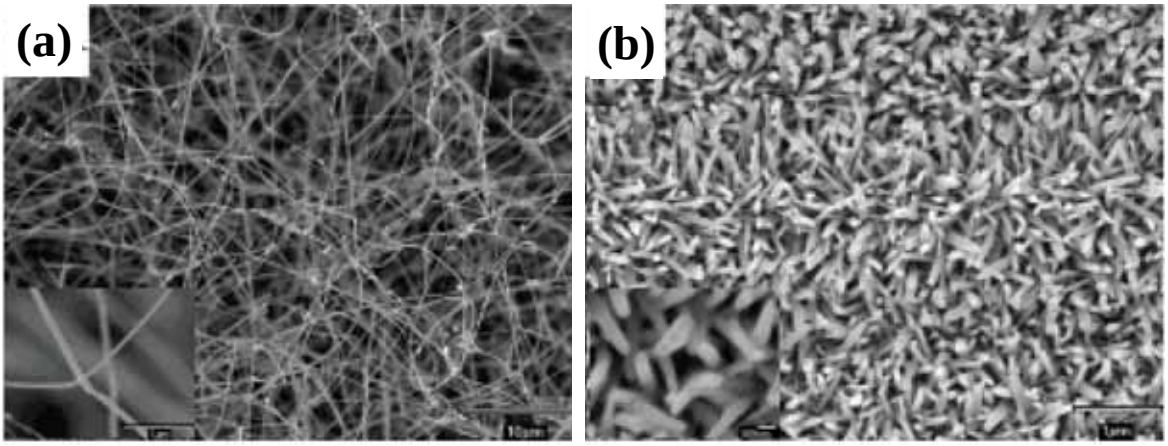

Figure 2-13 *(a) SEM image of the AgTCNQ nanowires. The inset is its higher magnification image. (b) SEM image of the CuTCNQ nanowires. The inset is its higher magnification image. [99]*

2.5 Field Emission Theory

Field emission is the process whereby electrons tunnel through a potential barrier into vacuum in the presence of a high electric field. This quantum mechanical tunneling process is highly dependent on material properties and shape of the emitter [100]. Surface imperfections, e.g. sharp needles, of the emitter can converge equipotential lines and that result in a stronger local field at the surface of the emitter [101, 102]. As the field turns strong enough, electrons can be extracted from the cathode material and emit into vacuum. Those electrons in vacuum are freely accelerated toward the anode, generating a current in the circuit.

To calculate the emission current, the tunnel probability were derived from the time independent Schrödinger equation [103]:

$$-\frac{\hbar}{2m^*}\frac{d^2\Psi}{dx^2}+V(x)\,\Psi=E\Psi \tag{2.30}$$

which can be rewritten as

$$\frac{d^2\Psi}{dx^2}=\frac{2m^*(V-E)\Psi}{\hbar^2} \tag{2.31}$$

Assuming that $V(x)$-E is independent of position in a section between x and $x+dx$, this equation can be solved yielding:

$$\Psi(x+dx) = \Psi(x)\exp(-kdx) \quad \text{with} \quad k = \frac{\sqrt{2m^*[V(x)-E]}}{\hbar} \tag{2.32}$$

The minus sign is chosen since the particle is assumed to move from left to right. For a slowly varying potential the amplitude of the wave function at $x = L$ can be related to the wave function at $x = 0$:

$$\Psi(L) = \Psi(0)\exp\left(-\int_0^L \frac{\sqrt{2m^*[V(x)-E]}}{\hbar}dx\right) \tag{2.33}$$

This equation is referred to as the WKB (Wentzel-Kramers-Brillouin) approximation.

$\Psi(x) = \exp(\Theta(x))$, and barrier $V(x) - E = q\phi_B(1 - x/L)$

From this the tunneling probability, Θ, can be calculated for a triangular barrier as

$$\Theta = \frac{\Psi(L)\Psi^*(L)}{\Psi(0)\Psi^*(0)} = \exp\left[-2\int_0^L \frac{\sqrt{2m^*}}{\hbar}\sqrt{q\Psi_B\left(1-\frac{x}{L}\right)}\,dx\right] \tag{2.34}$$

the tunneling probability then becomes

$$\Theta = \exp\left(-\frac{4}{3}\frac{\sqrt{2qm^*}}{\hbar}\frac{\phi_B^{3/2}}{F}\right) \tag{2.35}$$

where the electric field equals $F = \phi_B / L$.

The tunneling current is obtained from the product of the carrier charge, velocity and density. The velocity equals the Richardson velocity (v_R), the velocity with which on average the carriers approach the barrier while the carrier density equals the density of available electrons (n) multiplied with the tunneling probability (Θ), yielding:

$$J_n = qv_R n\,\Theta \tag{2.36}$$

which leads to:

$$J = K_1 F^2 \exp\left(\frac{K_2 \phi^{3/2}}{F}\right) \tag{2.37}$$

The tunneling current therefore depends exponentially on the barrier height to the 3/2 power. Generally, the field emission current (I) is measured as a function of the applied voltage (V). Substituting relationships of $J = I/A$ and $F = \beta V/d$ into Equation (2.37), where A is the emitting area, β is the local field enhancement factor at the emitting surface, and d is the distance between cathode and anode, following equation can be obtained:

$$\frac{I}{A} = K_1 \left(\frac{V}{d}\right)^2 \beta^2 \exp\left(\frac{K_2 \phi^{3/2} d}{\beta V}\right) \tag{2.38}$$

Rearrange Equation (2.38) and make the Napierian logarithm, yielding

$$\ln\left(\frac{I}{V^2}\right) = \ln\left[\frac{AK_1\beta^2}{d^2}\right] + \frac{K_2 d \phi^{3/2}}{\beta V} \tag{2.39}$$

Here, a plot of ln (I/V^2) versus $1/V$ yields a linear curve. This plot is the well-known Fowler-Nordheim (*FN*) plot [104]. The slope (S) of the linear curve in *FN* plot is given by

$$S = -\frac{K_2 d \phi^{3/2}}{\beta} \tag{2.40}$$

The value of field enhancement factor (β) can be estimated from the slope of the measured *FN* curve if the work function of the emitter is known. The larger the β, the higher the field concentration, and therefore the lower the effective threshold voltage for emission [105].